Determination of the Composition of TiN_x and TiB_xN_y Films by AES

M. A. Baker, J. Haupt, and W. Gissler

Institute of Advanced Materials Joint Research Center of the Commission of the European Communities, I-21020 Ispra (VA), Italy, Fax: +39-3 32-78 50 36

Z. Naturforsch. **50 a**, 624–630 (1995); received December 9, 1994

Dedicated to Prof. W. Müller-Warmuth on the occasion of his 65th birthday

For the determination of x and y of TiN_x and TiB_xN_y coatings two Auger methods are presented, one circumventing and the other minimising the difficulties arising from the overlap of the $KL_{23}L_{23}$ and $L_3M_{23}M_{23}$ peaks of N and Ti, respectively. The first method, developed for TiN_x coatings, is based on the $L_3M_{23}M_{45}$ valence band peak of Ti which develops a distinct second peak on nitridation, 3.9 eV below the main peak, labelled the L_3M_{23}Hybrid peak. After a simple Shirley background correction, a linear dependence of the L_3M_{23}Hybrid/$L_3M_{23}M_{45}$ peak height ratio on the N/Ti ratio was found. This allows the determination of the N content of a TiN_x compound. For TiB_xN_y coatings, a more complex shape of the $L_3M_{23}M_{45}$ peak is obtained due to the presence of more than one phase, rendering this peak unusable for quantification. Therefore the N/Ti ratio is obtained from the $L_3M_{23}M_{23}/L_3M_{23}M_{45}$ peak intensity ratio for Ti. To minimise influences of the fine structure and improve the accuracy of the method, the negative peak excursions were artificially broadened. The N/Ti ratio so obtained is used in combination with the B concentration determined from the $KL_{23}L_{23}$ peak of B to yield the Ti–B–N composition.

Introduction

There is a technological drive to develop materials with improved wear and corrosion properties. In the field of wear resistant coatings, the parameters of prime importance are hardness, toughness and corrosion resistance, which are all strongly dependent on the chemical composition. Titanium nitride is regarded at present as one of the most important technical coatings. It exhibits exceptional wear and corrosion resistance properties, has good electrical conductivity, a high melting point, and an attractive golden colour. The coating has many applications, primarily as a wear/corrosion resistant layer on cutting tools, but also as a diffusion barrier in semiconductor devices and as decorative coating. Titanium boron nitride is a coating in the development stage, offering very high hardness in combination with very low friction. Investigation of the chemical composition and microstructure yielding the best properties is the subject of the present research. Much work has of been undertaken to establish a simple and accurate method for the determination of the composition of TiN_x films. Many techniques, principally Auger Electron Spectroscopy (AES), X-ray Photoelectron Spectroscopy (XPS), Rutherford Backscattering Spectroscopy (RBS) and Energy Dispersive X-ray Analysis (EDX) have been considered [1–8]. None of the techniques is ideally suited. The low Rutherford scattering cross-section of N and the lowering of the signal/noise ratio with decreasing film thickness limits the accuracy of the RBS technique. EDX also has a large escape depth and this, combined with the overlap of the Ti Ll and N Kα lines and the low probability of the N Kα emission causes difficulties with quantification. The more surface sensitive electron spectroscopic techniques are normally prefered for thin film analysis, but for TiN_x problems of peak overlap and peak fitting in AES and XPS, respectively, have resulted in many different approaches [1, 2, 5, 6, 8]. For XPS, the unusual structure in the Ti 2p region between the Ti $2p_{1/2}$ and Ti $2p_{3/2}$ lines has been ascribed to satellite structure or the presence of oxygen which varies as a function of N concentration, causing uncertainties in the peak area measurements [1, 6–8]. Different background subtraction methods and peak fitting approaches have been applied in an attempt to circumvent this problem.

In AES, the overlap between the N–$KL_{23}L_{23}$ and the Ti–$L_3M_{23}M_{23}$ peaks necessitates an appropriate subtraction method with a secondary Ti peak in order to obtain the N–$KL_{23}L_{23}$ peak intensity. However, the Ti–$L_3M_{23}M_{45}$ peak, not interfering with N, has been observed to undergo substantial peak shape changes on nitridation and oxidation [9, 10]. In this paper these peak shape changes are investigated in detail for a range of TiN_x compositions. The electronic

Reprint requests to Dr. J. Haupt.

0932-0784 / 95 / 0700-0624 $ 06.00 © – Verlag der Zeitschrift für Naturforschung, D-72027 Tübingen

structure modification causing the observed peak shape changes will be interpreted, and a new method for the determination of the N/Ti ratio using the $L_3M_{23}M_{45}$ peak shape changes will be presented. As none of the analytical methods is ideally suited for the determination of the N content, the Ti/N ratio of the sample set obtained previously in this laboratory by XPS will be taken as reference.

For the ternary Ti–B–N system, the complexity of the Ti–$L_3M_{23}M_{45}$ peak shape changes precludes the use of this peak for quantification. The N/Ti ratio must be extracted from the overlapping Ti–$L_3M_{23}M_{23}$ and N–$KL_{23}L_{23}$ peaks. In a report of a "round robin" study, Perry et al. have summarised 4 different methods which have been used by authors in an attempt to correctly determine the N/Ti ratio from spectra acquired in the derivative mode [2]. Some of these methods make the assumption that peak shape changes arising from differing TiN ratios do not affect the positive or negative excursions used for quantification. Palmer has suggested that smoothing of high energy resolution data is a useful method to reduce the errors induced by lineshape distortions [4]. This technique will be considered for the determination of the N/Ti ratio of Ti–B–N samples. Quantification of all three elements can then be performed using the B–$KL_{23}L_{23}$ peak in conjunction with the obtained N/Ti ratio.

Experimental

TiN_x samples of varying stoichiometry were grown by reactive ion beam sputtering. Films with a thickness of 300–500 nm were deposited onto glass substrates. The preparation conditions have been described in detail in [11], and we have used samples and results described in that paper. The N/Ti ratio was evaluated there by XPS from the ratio of the areas under the N 1s and Ti 2p peaks, and the results were calibrated against a stoichiometry reference sample.

A novel method was used in the preparation of the sputter deposited Ti–B–N films, enabling a variation of the Ti/B ratio within the sample set. Onto a BN target, 0.7 × 0.7 mm titanium pieces were mounted at regular spacings. To produce a range of Ti–B–N compositions, the ratio of Ti/BN coverage was progressively increased by reducing the spacing.

Auger analysis was performed on a Riber Nanoscan 50 spectrometer. An incident beam voltage of 5 keV and current of 80–120 nA was employed. Measurements were taken with the MAC2 analyser operating at constant analyser energy (CAE mode). For the TiN_x samples, a high energy resolution of 0.5 eV and step width of 0.1 eV was employed to obtain well resolved spectra of the Ti–$L_3M_{23}M_{45}$ peak region. An energy resolution of 3 eV and step width of 0.5 eV was used to obtain the Ti–B–N wide scan spectra. The spectrometer was calibrated with an Al X-ray source and the Cu $2p_{3/2}$ and Cu 3p peaks referenced to the Fermi level at 932.67 and 75.14 eV, respectively [12]. Prior to analysis, the samples were sputtered using an argon ion gun rastered over an area of 0.7 mm^2, operating at an incident beam voltage of 3 keV and 0.2 μA. The Auger analysis was taken with a rastered beam from the central region of the crater, over an area of <0.1 mm^2. In order to study the Ti peak shape in detail it is particularly important to completely remove the native oxide by etching. Figure 1 shows the reduction of the oxygen peak intensity on the surface of Ti and $TiN_{1.06}$ as a function of etch time. After an etch of 150 seconds, the oxide from both samples has been removed and a bulk signal is obtained. For uniformity and possible preferential sputtering effects, an etch time of 150 seconds, prior to analysis, was employed for all samples examined.

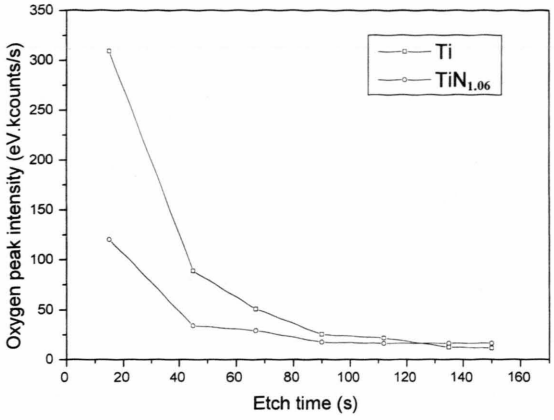

Fig. 1. Oxygen peak intensity as function of Ar ion etch time (energy 3 keV; 0.2 μA).

Results

1. *TiN_x Samples*

Figure 2 shows changes in the Ti–$L_3M_{23}M_{45}$ spectral region with increasing N concentration. The $L_3M_{23}M_{45}$ peak present in the pure Ti spectrum de-

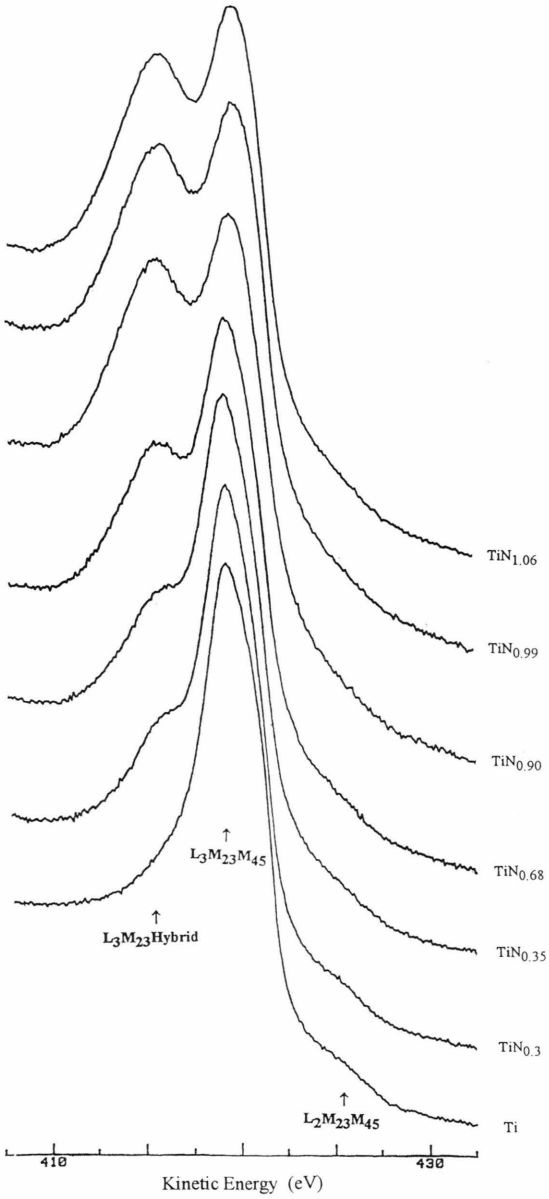

Fig. 2. Ti–$L_3M_{23}M_{45}$ direct mode high resolution raw spectra for various N concentrations from 0 to 1.06.

creased in amplitude, with no substantial change in peak position as the N content increased. As a consequence of Ti–N bond formation a second peak emerges about 4 eV below the main peak, which grows with increasing N concentration. A description and interpretation of these peak shape changes on nitridation has not been reported in the literature and so will be considered in the following section.

1.1 Interpretation of the Ti LMM peak shape changes on nitridation

The M_{23} level for Ti has a binding energy of 34.6 eV [13] and exhibits properties of a core level, whereas the M_{45} level refers to the 3d valence band. The $L_3M_{23}M_{45}$ transition for Ti reflects the Ti partial density of states in the valence band, and changes in this peak should be relatable to valence band calculations for Ti in different environments. The d-band DOS calculations for Ti and TiN have been reported by Hygh and Welch [14] and Neckel et al. [15], respectively, and the latter are shown in Figure 3. The calculations of Hygh and Welch indicate the presence of a single peak in the DOS within 1.5 eV from E_f.

In the $L_3M_{23}M_{45}$ spectrum recorded here for Ti there is a single peak at 419.2 eV. For Ti in TiN, the DOS calculated by Neckel et al. show that the presence of N has caused a substantial rearrangement of the d state density (Ti 3d partial DOS), with a considerable number of electrons being drawn to a higher binding energy, the maximum lying very close to 5 eV. This new electron density maximum should be evident in the Ti–$L_3M_{23}M_{45}$ spectral region for TiN and is clearly the origin of the secondary peak at lower kinetic energy in Figure 2. This transition has been assigned as the L_3M_{23}Hybrid peak and occurs in the raw data at 3.9 eV below the $L_3M_{23}M_{45}$ valence band peak. (The $L_3M_{23}M_{45}$ peak position shifts to 419.5 eV on nitridation and for the $TiN_{1.06}$ spectrum after an approximate peak overlap deconvolution, the

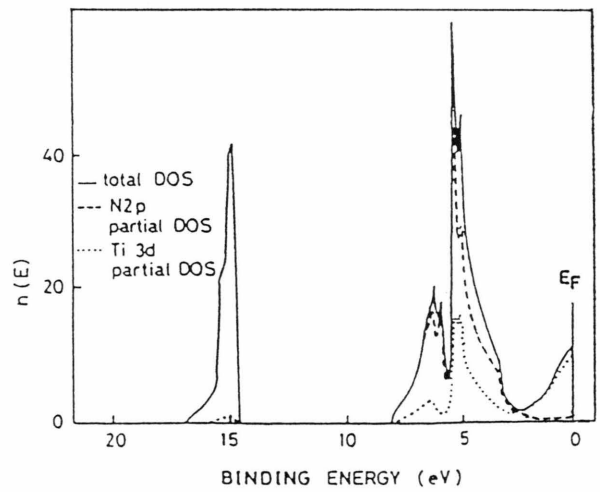

Fig. 3. DOS calculation for TiN (taken from Neckel et al. [15]). For the Auger Ti–$L_3M_{23}M_{45}$ peak only the Ti 3d partial DOS has to be considered.

peak separation increases to 4.25 eV, in excellent agreement with the calculated data.) It can be seen from the predicted DOS and the XPS/UPS measurements of Porte et al. [16] and Johansson et al. [17] that the electrons at higher binding energy combine with the N 2p electrons to form a strong hybrid orbital, which is the cause of many of the extraordinary properties of this material. However, the DOS calculation predicts that a significant fraction of the d electrons remains close to the Fermi level, giving rise to the excellent electrical conduction properties of the material and explaining the continued presence of the $L_3M_{23}M_{45}$ peak in the spectra for TiN.

1.2 Determination of the N/Ti ratio

The distinctive change in the structure around the LMM peak clearly provides a potential source of information from which the N/Ti ratio can be found. The determination of intensities is best performed by measurement of peak areas, but the complex peak structure and undetermined transition probabilities make this approach untenable. Consequently, quantification of intensity was performed by measuring peak heights after subtracting the background. The step like nature of the background in the Auger spectrum for the recorded peak set enables the use of a simple Shirley background subtraction. In order to have a direct relation of the measured raw data with the N content, the intensity at the position of the two peak centres was taken, and the L_3M_{23}Hybrid/$L_3M_{23}M_{45}$ peak height ratio (expressed as a percentage) as a function of the N/Ti ratio was plotted in Figure 4. The N/Ti ratio was previously determined using XPS [11]. It can clearly be seen that the peak height ratio depends linearly on the N content. This has the interesting implication that the number of d electrons extracted from the metallic bonding to be involved in the formation of the hybrid orbital varies linearly with N concentration. The offset at N/Ti = 0 is due to a contribution from the peak tail of the pure Ti sample at the hybrid peak position.

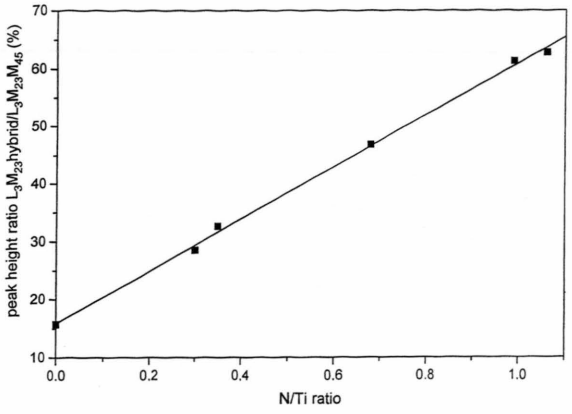

Fig. 4. Peak height ratio after a Shirley background correction of the Auger raw data peaks (L_3M_{23}Hybrid/$L_3M_{23}M_{45}$ in %) as function of the N/Ti ratio determined by XPS [11]. The offset at N/Ti = 0 is due to the long tail of the pure Ti line.

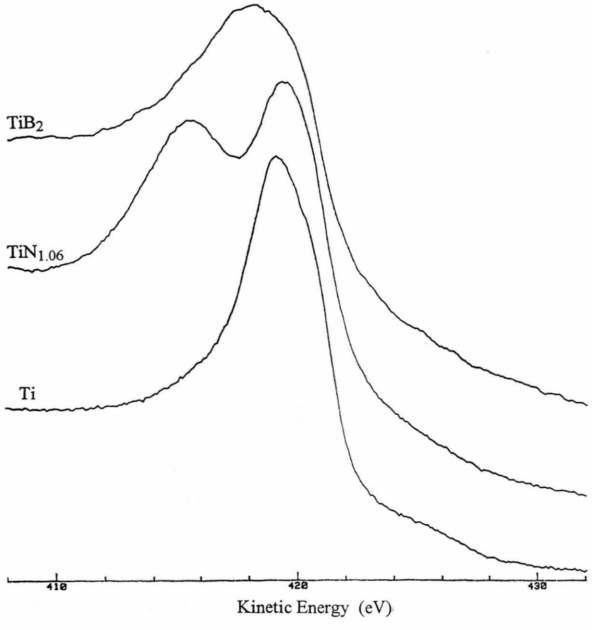

Fig. 5. The Auger Ti–$L_3M_{23}M_{45}$ peak for TiB_2, $TiN_{1.06}$ and Ti.

2. *Ti–B–N Samples*

For the quantification of Ti–B–N samples, the Ti/N peak overlap remains problematic, and use of the Ti–$L_3M_{23}M_{45}$ peak is again attractive. However, the tertiary Ti–B–N system is more complex with the possible presence of many different phases [18]. The predominant phases for Ti–B–N compositions showing good mechanical properties are TiN and TiB_2 [19]. Figure 5 shows standard spectra taken of Ti, $TiN_{1.06}$, and TiB_2. From these spectra it can be seen that, when both TiN and TiB_2 are present in the same material, a more complex peak shape will be obtained with no clear separation of the peak components,

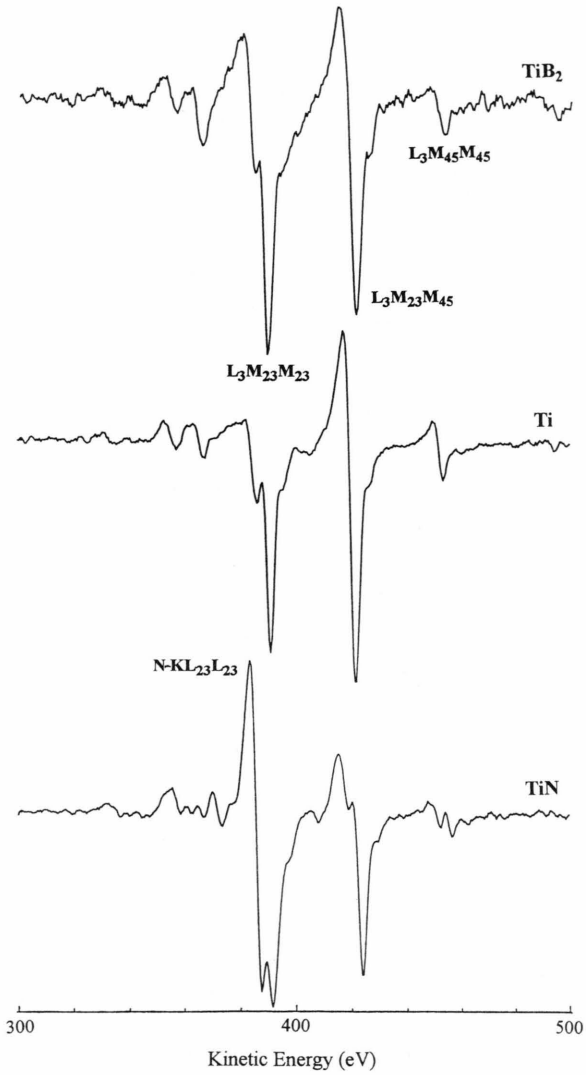

Fig. 6. Differentiated spectra for Ti, TiN and TiB_2.

making the use of the Ti–$L_3M_{23}M_{45}$ peak shape changes untenable as a simple quantification method.

Many other methods have been suggested for determining the Ti/N ratio from the Ti–LMM peak set recorded for TiN_x samples. Palmer has reviewed many of these methods and mentioned the important point that the lineshape of the three peaks in the Ti–L_3MM triplet are affected by changes in chemical state, making the use of spectral subtraction as a means of extracting one peak from two overlapping peaks, potentially erroneous [4]. Differentiated spectra for Ti, TiN and TiB_2 are shown in Figure 6. There is

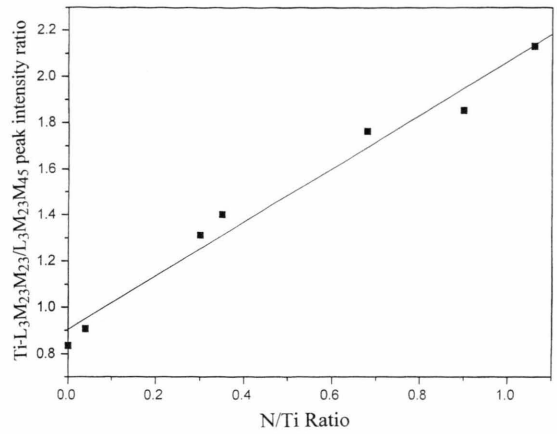

Fig. 7. Plot of the Ti–$L_3M_{23}M_{23}/L_3M_{23}M_{45}$ peak intensity ratio (negative excursions) as a function of N/Ti ratio determined by XPS [11].

a stronger positive excursion of the Ti–$L_3M_{23}M_{23}$ peak for TiB_2 compared with Ti, and the peak-to-peak ratio of the $L_3M_{23}M_{23}/L_3M_{23}M_{45}$ peaks is substantially different between the two materials. TiN, as seen in the previous section, has a strongly modified $L_3M_{23}M_{45}$ positive excursion. Degrading the energy resolution of the spectrum by smoothing can reduce the effect of line shape changes on quantification, as the contribution from the fine structure becomes folded into a standardised lineshape, the peak-to-peak measurement then being again proportional to the peak area. This method is described in detail by Palmer [4]. Consequently, for potential use in quantification of Ti–B–N spectra, this procedure was tested for smoothing wide scan spectra of TiN_x samples of varying stoichiometry, many of which were used in the TiN_x study described in Section 1. A combination of a 25 point smooth and 25 point differentiation was found to remove the fine structure.

For determination of the Ti/N ratio, Palmer used the ratio of the Ti–$L_3M_{23}M_{23}$ + N–$KL_{23}L_{23}$ (negative excursion)/Ti–$L_3M_{23}M_{45}$ (peak-to-peak). However, for the samples examined here, a slightly better fit to a linear function was obtained for the ratio Ti–$L_3M_{23}M_{23}$ + N–$KL_{23}L_{23}$ (negative excursion)/Ti–$L_3M_{23}M_{45}$ (negative excursion). The results and calibration curve are shown in Figure 7. With the calibration curve, it is now a simple procedure to obtain the N/Ti ratio. The B–$KL_{23}L_{23}$/Ti–$L_3M_{23}M_{45}$ sensitivity factor was determined from a TiB_2 standard, and using this factor, the stoichiometric TiB_xN_y composition can then be calculated.

Discussion

The new Ti–L_3M_{23}Hybrid/$L_3M_{23}M_{45}$ peak height ratio method described for TiN_x stoichiometric determination has the following advantages:

(i) only a single peak need be recorded;
(ii) little data processing is required;
(iii) after simple determination of the peak height ratio, the Ti/N ratio can be immediately read from the calibration curve;
(iv) information regarding the bonding of Ti can be extracted from each data set;
(v) inherent errors in Ti–$L_3M_{23}M_{23}$/$L_3M_{23}M_{45}$ peak subtraction/ratio methods due to peak shape changes are avoided.

For Ti–B–N, the situation is more difficult as the N/Ti peak overlap problem is unavoidable. Employment of any Ti–$L_3M_{23}M_{23}$/$L_3M_{23}M_{45}$ peak intensity ratio method to obtain the Ti/N ratio from Ti–B–N samples is potentially erroneous, as it assumes that the presence of TiB_2 in addition to TiN does not change the Ti peak intensity ratio. However, use of the smoothed negative excursions to establish the N/Ti ratio for Ti–B–N samples does have two advantages. Firstly, the $L_3M_{23}M_{45}$ positive excursion and its substantial peak shape changes are avoided which, even after smoothing, probably show a non-linear variation through the range of TiN_x compositions. Secondly, the presence of TiB_2 in addition to TiN leads to an increase in the positive excursion of the Ti–$L_3M_{23}M_{23}$ peak. If the peak-to-peak instead of the negative excursion had been used for construction of the calibration curve, then in the presence of TiB_2, the N/Ti value read from the curve would be underestimated.

The scatter of results from the Ti–$L_3M_{23}M_{23}$/$L_3M_{23}M_{45}$ peak ratio calibration curve is larger than those obtained from the high energy resolution L_3M_{23}Hybrid/$L_3M_{23}M_{45}$ peak-height ratio method. Consequently, the peak-height ratio method should be used for accurate TiN_x composition determination. The difficulties with quantifying Auger spectra for Ti–B–N combined with the larger uncertainty in the accuracy of the result would favour the consideration of other analytical methods for simple composition determination, in spite of the rapid acquisition time for AES. For depth profiling studies, where substantial variations in the elemental composition with depth (and not the absolute composition) is the most important parameter to be studied, the method described above is recommendable. We have found XPS to give reliable composition values and important extra chemical state information regarding Ti–B–N films [20].

Conclusions

The quantification of Auger spectra for the important thin film materials TiN_x and TiB_xN_y has been considered. For TiN_x, high energy resolution Auger spectra of the $L_3M_{23}M_{45}$ region have shown the growth with nitridation of a clearly resolvable secondary peak at approximately 4 eV below the main peak. The observed peak structure changes have been compared with theoretical valence band calculations, enabling an interpretation and discussion of the origin of the secondary peak and its assignation as an L_3M_{23}Hybrid transition. A plot of the L_3M_{23}Hybrid/$L_3M_{23}M_{45}$ peak height ratio as a function of N content shows a linear dependence. It is proposed that the substantial changes in Ti–$L_3M_{23}M_{45}$ valence band peak on nitridation of Ti be used as a new method of calculating the Ti/N ratio for TiN_x samples of unknown stoichiometry.

Ti–B–N films exhibit at least two phases. TiN and TiB_2 are predominant in compositions showing interesting wear and corrosion resistant properties. The presence of these two phases produces a more convoluted Ti–$L_3M_{23}M_{45}$ peak shape than for TiN_x, precluding its use for quantification. The overlapping Ti–$L_3M_{23}M_{23}$ and N–$KL_{23}L_{23}$ peaks must be used for quantification. After smoothing the data to remove the peak fine structure, a plot of the Ti–$L_3M_{23}M_{23}$/$L_3M_{23}M_{45}$ peak ratio (negative excursions) against the N/Ti ratio provides a calibration curve from which the N/Ti ratio can be determined. This method of N/Ti ratio determination was found to be less accurate than the L_3M_{23}Hybrid/$L_3M_{23}M_{45}$ peak height ratio method. For accurate absolute Ti–B–N composition determination, AES is not recommended, but is advisable for following substantial composition variations in depth profiling studies.

[1] S. Hofmann, J. Vac. Sci. Tech. A **12,** 2789 (1986).
[2] A. J. Perry, C. Strandberg, W. D. Sproul, S. Hofmann, C. Ernsberger, J. Nickerson, and L. Chollet, Thin Solid Films **153,** 169 (1987).
[3] J. E. Sundgren, A. Rockett, J. E. Greene, and U. Helmersson, J. Vac. Sci. Tech. A **4,** 2770 (1986).
[4] W. Palmer, Surface and Interface Analysis **13,** 55 (1988).
[5] P. T. Dawson and K. K. Tzatzov, Surface Science **149,** 105 (1985).
[6] B. J. Burrow, A. E. Morgan, and R. C. Ellwanger, J. Vac. Sci. Tech. A **4,** 2463 (1986).
[7] N. Heide, B. Siemensmeyer, and J. W. Schulze, Surface and Interface Analysis **19,** 423 (1992).
[8] K. S. Robinson and P. M. A. Sherwood, Surface and Interface Analysis **6,** 261 (1984).
[9] F. Pellerin, C. Bodin, and T. Pech, J. Vac. Sci. Tech. A **5,** 1371 (1987).
[10] B. Minh Duc, C. Jardin, J. P. Gauthier, G. Thollet, and P. Michel, J. Electron Spectroscopy and Related Phenomena **20,** 213 (1980).
[11] R. C. Buschert, P. N. Gibson, W. Gissler, J. Haupt, A. Manara, X. Jiang, and K. Reichelt, Surface and Interface Analysis **16,** 510 (1990).
[12] M. P. Seah and G. C. Smith, in Practical Surface Analysis, Vol. 1 2nd Edition, Ed. D. Briggs and M. P. Seah, John Wiley, Chichester, U.K. 1990, Appendix 1, p. 531–540.
[13] K. D. Sevier, Low Energy Electron Spectrometry, Wiley-Interscience, London 1972, Appendix F.
[14] E. H. Hygh and R. M. Welch, Phys. Rev. B **1,** 2424 (1970).
[15] A. Neckel, P. Rastl, R. Eibler, P. Weinberger, and K. Schwarz, J. Phys. C: Solid State Phys. **9,** 579 (1976).
[16] L. Porte, L. Roux, and J. Hanus, Phys. Rev. **28,** 3214 (1983).
[17] L. I. Johansson, P. M. Stefan, M. L. Shek, and A. Norlund Christensen, Phys. Rev. B **22,** 1032 (1980).
[18] H. Novotny, F. Benesovsky, C. Brukl, and O. Schob, Mh. Chem. **92,** 403 (1961).
[19] P. Hammer, A. Steiner, R. Villa, M. A. Baker, P. N. Gibson, J. Haupt, and W. Gissler, of Surface and Coatings Technology, **68/69,** 194 (1994).
[20] M. A. Baker, A. Steiner, J. Haupt, and W. Gissler, of presented at the 41st, National Symposium of the American Vacuum Society, Denver U.S.A., October 1994.